Title

Melanoma dedifferentiation induced by interferon-gamma epigenetic remodeling in response to anti-PD-1 therapy

Journal

Journal of Clinical Investigation, 131(12)

ISSN

0021-9738

Authors

Kim, Yeon Joo
Sheu, Katherine M
Tsoi, Jennifer
et al.

Publication Date

2021-06-15

DOI

10.1172/jci145859

Peer reviewed

Title: Melanoma dedifferentiation induced by interferon-gamma epigenetic remodeling in response to anti-PD-1 therapy

Authors: Yeon Joo Kim[1,2], Katherine M. Sheu[1,3], Jennifer Tsoi[1], Gabriel Abril-Rodriguez[1,2], Egmidio Medina[1], Catherine S. Grasso[4], Davis Y. Torrejon[1], Ameya S. Champhekar[1], Kevin Litchfield[5], Charles Swanton[5,6], Daniel E. Speiser[7], Philip O. Scumpia[1], Alexander Hoffmann[3], Thomas G. Graeber[2,8,9], Cristina Puig-Saus[1,8,10], Antoni Ribas[1,2,8,10,11]

Affiliations: 1. Department of Medicine, University of California, Los Angeles (UCLA). 2. Department of Molecular and Medical Pharmacology, UCLA. 3. Department of Microbiology, Immunology, and Molecular Genetics, UCLA**.** 4. Department of Surgery, Cedars-Sinai Medical Center, Los Angeles, CA, USA. 5. Cancer Research UK Lung Cancer Centre of Excellence, University College London Cancer Institute, London, UK**.** 6. Cancer Evolution and Genome Instability Laboratory, The Francis Crick Institute, London, UK. 7. University of Lausanne, Switzerland**.** 8. Jonsson Comprehensive Cancer Center, Los Angeles, CA 90095, USA. 9. Crump Institute for Molecular Imaging, Los Angeles, CA 90095, USA**.** 10. Parker Institute for Cancer Immunotherapy, San Francisco, CA 94129, USA. 11. Department of Surgery, Division of Surgical Oncology, UCLA.

Correspondence: Antoni Ribas, M.D, Ph.D., Department of Medicine, Division of Hematology-Oncology, 11-934 Factor Building, Jonsson Comprehensive Cancer Center at UCLA, 10833 Le Conte Avenue, Los Angeles, CA 90095-1782, USA. Telephone: 310-206-3928. Fax: 310-825-2493. E-mail: aribas@mednet.ucla.edu.

Conflict of Interest Statement: K.L. reports speaker fees from Roche Tissue Diagnostics. C.S. reports grant support from Pfizer, AstraZeneca, BMS, Roche-Ventana, Boehringer-Ingelheim,

and Ono. C.S. has consulted for Pfizer, Novartis, GlaxoSmithKline, MSD, BMS, Celgene, AstraZeneca, Illumina, Genentech, Roche-Ventana, GRAIL, Medicxi, and the Sarah Cannon Research Institute. C.S. is a shareholder of Apogen Biotechnologies, Epic Bioscience, GRAIL, and has stock options in and is co-founder of Achilles Therapeutics. T.G.G. reports receiving an honorarium from Amgen, and having consulting and equity agreements with Trethera Corporation. The lab of T.G.G. has completed a research agreement with ImmunoActiva. A.R. has received honoraria from consulting with Amgen, Bristol-Myers Squibb, Chugai, Genentech, Merck, Novartis, Roche and Sanofi, is or has been a member of the scientific advisory board and holds stock in Advaxis, Apricity, Arcus Biosciences, Bioncotech Therapeutics, Compugen, CytomX, Five Prime, FLX-Bio, ImaginAb, Isoplexis, Kite-Gilead, Lutris Pharma, Merus, PACT Pharma, Rgenix and Tango Therapeutics, has received research funding from Agilent and from Bristol-Myers Squibb through Stand Up to Cancer (SU2C).

Abstract

Melanoma dedifferentiation has been reported as a state of cellular resistance to targeted therapies and immunotherapies as cancer cells revert to a more primitive cellular phenotype. Here we show that, counterintuitively, the biopsies of patient tumors that respond to anti-programmed cell death receptor 1 (PD-1) therapy decreased expression of melanocytic markers and increased neural crest markers, suggesting treatment-induced dedifferentiation. When modeling the effects *in vitro*, we documented that melanoma cell lines that were originally melanocytic differentiated underwent a process of neural crest dedifferentiation when continuously exposed to interferon gamma, through global chromatin landscape changes leading to enrichment in specific hyperaccessible chromatin regions. The interferon gamma-induced dedifferentiation signature corresponded with improved outcomes in patients with melanoma, challenging the notion that neural crest dedifferentiation is entirely an adverse phenotype.

Brief Summary

Successful PD-1 blockade therapy is associated with an interferon-induced melanoma dedifferentiation mediated by epigenetic reprogramming of cancer cells

Introduction

Cancer immunotherapy has remarkably improved the treatment landscape for patients with advanced melanoma. Melanoma is the result of a malignant transformation of melanocytes, which develop from neural crest cells during embryogenesis (1, 2). The melanoma cancer cells arise from different stages of differentiation between the neural crest precursors and fully differentiated melanocytes (2-6). Not only are melanomas highly heterogeneous, they also display a large degree of plasticity that is highlighted by the ability of the differentiated cancer cells to dedifferentiate to a more neural crest phenotype. Melanoma dedifferentiation is defined by the loss of melanosomal antigens such as the melanoma antigen recognized by T cells 1 (MART-1/ Melan-A) or gp100, with the concomitant gain of neural crest markers such as the nerve growth factor receptor (NGFR or CD271) or AXL (5, 7, 8). The expression of the melanosomal antigens is driven by the microphthalmia associated transcription factor (MITF), the master regulator of melanoma differentiation (9, 10). Therefore, the downregulation of MITF is a major feature of dedifferentiation. This phenotypic plasticity has been associated with therapeutic resistance to BRAF inhibitors, being a feature of drug-resistant cells that persist after the majority of other cells have been eliminated by the targeted therapy (5, 6, 8, 11, 12). It has also been shown to be a resistance mechanism against melanocytic antigen-specific T cell adoptive cell transfer therapy in both mice (13) and humans (14). Furthermore, the pro-inflammatory cytokine tumor necrosis factor (TNF) was shown to induce this dedifferentiation (13, 14). The TNF-induced dedifferentiation was reversible with the removal of immune stimulation (14), suggesting that epigenetic and transcriptomic mechanisms may be at play.

Despite the multitude of studies on melanoma plasticity, its role in the context of immune checkpoint blockade therapy has not been elucidated. In fact, indirect evidence has led to the postulation that dedifferentiation would be a state of resistance to immunotherapy for melanoma

(15-17). Therefore, we investigated whether melanocytic dedifferentiation was associated with therapeutic response or resistance to PD-1 blockade therapy in patients with advanced melanoma.

Results

Loss of melanocytic lineage markers is associated with clinical response to immune checkpoint blockade

To study the effect of melanocyte lineage differentiation state, we analyzed baseline and on-therapy biopsies of patients receiving immune checkpoint blockade (ICB) therapy from the CheckMate 038 clinical trial (18, 19). This was a prospective, multicenter, international, multi-cohort clinical trial designed to collect tumor biopsies from patients with metastatic melanoma treated with the anti-PD-1 antibody nivolumab as front-line therapy or after progressing on therapy with the anti-cytotoxic T cell antigen 4 (CTLA-4) antibody ipilimumab, or receiving the combination of both antibodies (18, 19). Of the 101 patients, 68 had paired biopsies, and of those paired, 27 were from patients with progressive disease (PD), 14 with stable disease (SD), and 27 with complete response or partial response (CRPR). On-therapy biopsies, collected at approximately one month after starting on ICB therapy had notable downregulation of *MITF* and *MLANA* and concomitant upregulation of *AXL* only from the CRPR group. The biopsies from the SD and PD groups did not display significant changes in *MITF*, *MLANA*, or *AXL* following treatment (Figure 1). This observation is at odds with the conventional view of dedifferentiation as a resistance mechanism (17), and indicates that dedifferentiation may serve as a marker of favorable response to immune checkpoint blockade. As the presence of interferon-gamma (IFNγ) signatures in biopsies is best correlated with response to the anti-PD-1 therapy (19-21), we hypothesized that the dedifferentiation of these responding tumors may be mediated by continued exposure to T cells producing IFNγ.

In vitro modeling of cytokine-induced melanoma dedifferentiation

Previously, it has been reported that human melanoma cell lines can be categorized into four subtypes based on their differentiation states: Melanocytic, transitory, neural crest-like, and

undifferentiated (6). The cell lines that are baseline melanocytic differentiated, characterized by high expression of MART-1 and no expression of neural crest marker NGFR, have an ability to become dedifferentiated upon exposure to TNF or a BRAF inhibitor (6, 13). To test whether IFNγ induces this same phenotypic change, we established an *in vitro* system to model the phenotypic plasticity. Four baseline differentiated human melanoma cell lines (M262, M308, M399 and 3998mel) were treated continuously with human recombinant IFNγ and the change in phenotype was compared to the dedifferentiation induced by three days of TNF, which served as a positive control for melanoma dedifferentiation. Flow cytometry using fluorescent anti-MART-1 and anti-NGFR antibodies revealed dedifferentiation of these four cell lines over the course of two to five weeks (Figure 2A and Supplemental Figure 1A). The duration of continuous IFNγ exposure needed to reach the maximal MART-1-low, NGFR-high state varied for each cell line but were comparable to the approximate one-month time point at which the aforementioned biopsies were taken during the course of the anti-PD-1 therapy in patients. In addition, in four human melanoma cell lines that were baseline undifferentiated (M257A2, M370, M381 and M410), neither cytokines induced dedifferentiation. Interestingly, continuous IFNγ exposure led to what appears to be redifferentiation of some of these cell lines. The cells increased NGFR levels with no change in MART-1 levels, a reversal of the last step of the previously described melanoma dedifferentiation trajectory from neural crest-like to undifferentiated (Figure 2A and Supplemental Figure 1A) (6).

Concordant transcriptomic programs reflect the phenotypic plasticity driven by IFNγ and TNF

To study the mechanism of this cytokine-induced cellular plasticity, we performed whole transcriptome RNA sequencing (RNA-seq) and assay for transposase-accessible chromatin sequencing (ATAC-seq) on the aforementioned eight cell lines, four that were differentiated at baseline and dedifferentiate with IFNγ exposure, and four that were undifferentiated at baseline

and did not differentiate further with continuous IFNγ exposure, as well as the same cell lines exposed to three days of TNF as positive control (Figure 2A).

To assess the effect of cytokine treatment on the melanoma transcriptome, we projected all samples onto a previously defined principal component analysis (PCA) framework of 54 baseline human melanoma cell lines spanning the four defined differentiation states (6). As expected, the projection of the eight cell lines segregated according to the baseline differentiation status, with the dedifferentiated samples from either cytokine shifting towards a more neural crest-like state within the defined dedifferentiation trajectory (Figure 2B). We also interrogated the gene expression profiles of our samples for the enrichment of previously defined gene signatures for various melanoma differentiation states, from melanocytic (M) to undifferentiated (U). Clear downregulation of the melanocytic subtype signature was observed with either cytokine-driven dedifferentiation, with the concomitant enrichment of the neural crest or transitory subtype signatures (Figure 2C). There were no distinguishing patterns between the two groups of cell lines in terms of nonsense or missense mutations in well-studied, relevant genes that may contribute to the observed differences (Figure 2D). In addition, neither group harbored consequential mutations in genes that code for critical members of the IFNγ response pathway, as previously reported in melanoma tumors (22, 23), suggesting that these cell lines all activate IFNγ-dependent transcription factors upon stimulation (Supplemental Figures 1B and 2A-B).

In order to identify commonly induced genes across all cell lines, we performed partial least squares regression (PLSR) on baseline versus cytokine-exposed cell lines. All eight samples had clear cytokine responses regardless of their baseline differentiation status (Figure 3A and 3C), which ensures that the difference in phenotype is not attributable to any lack of cytokine response in one group. Ranking of the genes induced by continued IFNγ exposure across the eight cell lines revealed upregulation of *IRF1*, *SOSC1* and *STAT1* (Figure 3B and Supplemental Table 1).

The K-means clustering of the top 300 upregulated genes revealed a cluster of genes that were commonly induced to similar levels in both baseline-differentiated and undifferentiated lines upon continued IFNγ exposure (Figure 3B). It also revealed a distinct cluster of genes that were strongly induced in only the undifferentiated lines (Figure 3B), which suggests induction of a transcriptional response from these cell lines despite their already dedifferentiated state. The clusters of genes highly upregulated in the dedifferentiating group were also upregulated to similar levels in the baseline undifferentiated group, which indicates that the IFNγ downstream signaling is preserved regardless of the differentiation status and suggests that epigenetic differences not captured by the gene expression analysis may be responsible for the diverging plasticity. The ranking of genes induced by TNF across the eight cell lines pointed at much stronger upregulation of *TNF*, *TNFAIP3*, and *NFKBIA* in comparison to their rank in the IFNγ analysis (Figure 3D, Supplemental Table 1). The K-means clustering of the top 300 upregulated genes revealed a cluster of genes that were much more strongly induced in the samples that dedifferentiate, indicating a transcriptional program induced by TNF that is unique to cells capable of the phenotypic switch. We additionally looked at the cross enrichment of one cytokine with the top 300 induced genes from the other. The TNF matrix with the top 300 IFNγ -induced genes and the IFNγ matrix with the top 300 TNF-induced genes showed similar levels of induction (Supplemental Figures 2C-D).

To determine whether the IFNγ- and TNF-induced dedifferentiation states had similar gene expression profile changes, we performed rank-rank hypergeometric overlap (24). Significant overlap in IFNγ- and TNF-induced genes were revealed (Figure 3E), with an even higher degree of overlap at the level of gene sets (Figure 3F). This data indicates concordant gene programs despite the difference in inducible expression of individual genes. Examining the enrichment of the terms from GSEA, or GSEA-squared (25), confirmed the loss of pigmentation with the gain of inflammatory signaling following IFNγ and TNF exposures (Figure 3G and 3H, and Supplemental Table 2).

TNF and IFNγ induce dedifferentiation via distinct global chromatin landscape alterations

Evaluation of the ATAC-seq tracks at the promoter of *MLANA* revealed no basal chromatin accessibility in undifferentiated cell lines along with a decrease of chromatin accessibility of differentiated cell lines upon IFNγ- or TNF-induced dedifferentiation, consistent with the flow cytometry and RNA-seq data (Figure 4A). ATAC-seq tracks at the promoter of *AXL* also revealed the expected pattern, with no changes in the baseline undifferentiated cell lines upon cytokine exposure, and increased peaks in the baseline differentiated cell lines when they dedifferentiate upon cytokine exposure (Figure 4A). Pair-wise comparisons of cytokine-stimulated to unstimulated cell lines revealed between 2500 and 7000 peaks that were hyperaccessible following either IFNγ or TNF exposure (Figure 4B). Interestingly, IFNγ induced a similar number of hyperaccessible peaks for both the baseline differentiated and the undifferentiated cell lines, but TNF induced a large number of hyperaccessible peaks only in baseline differentiated cell lines (Figure 4B). Principal component analysis of all induced ATAC-seq peaks showed that the baseline differentiated and the undifferentiated cell lines exist in two different epigenomic states. TNF exposure in undifferentiated cell lines caused minimal epigenetic changes but drove drastic changes toward the undifferentiated state in the baseline differentiated ones, consistent with the transcriptional response (Figure 4C). The baseline differentiation states and the shared phenotypic change due to IFNγ and TNF were best represented by PC1, whereas PC2 best defined the divergence in the effects of the two cytokines, revealing the IFNγ-specific response. Despite inducing the comparable changes in NGFR and MART-1 status based on protein expression, the exposure to either of the two cytokines resulted in distinctive chromatin alterations which manifest as a shift along one or both axes of the PCA analysis. Of note, PC2 also supported the redifferentiation phenomenon (Figure 4C) observed in the flow cytometry data (Figures 2A and Supplemental Figure 1A).

K-means clustering of accessible chromatin peaks induced by either cytokine revealed that the changes in chromatin accessibility fell into three main patterns: IFNγ-inducible across the two baseline states, TNF-inducible but only in the differentiated cell lines, and common to both IFNγ and TNF but only in the undifferentiated cell lines where these regions are open at baseline (Figure 4D, Supplemental Figure 3A). This suggests the presence of a high baseline signaling pathway that may be responsible for the lack of further response to stimulation by TNF. Motif enrichment analysis of the ATAC peaks revealed distinct clusters of transcription factors whose binding sites were opened upon IFNγ or TNF exposure. Notably, no common motifs were enriched to comparable levels in the IFNγ- and TNF-induced peaks. The motifs of select IRF proteins were the most highly enriched following IFNγ, while the motifs of the ATF3, BATF, and AP-1 family factors were the most highly enriched following TNF, even more so than those of NFκB (Figure 4E and Supplemental Figure 3B). Both TNF and IFNγ exposures led to largely hyper-accessible chromatin in intergenic regions that were associated with axon guidance and cell migration (Figure 4F). However, their effects were distinct in that TNF opened chromatin regions near genes associated with mitogen-activated protein kinase (MAPK) pathway, neuronal system, and growth factor signaling, while IFNγ generated stronger enrichment for chromatin regions near genes involved in interferon response and antigen presentation (Figure 4F).

Motif enrichment analysis of hyper-accessible chromatin regions following IFNγ and TNF exposure reveal regulators involved in dedifferentiation

We next asked how the baseline differentiation states of the melanoma cell lines, their baseline epigenomic profiles and signaling network, affected their response to IFNγ stimulation. Although similar numbers of peaks were found to be inducible by IFNγ in baseline differentiated and undifferentiated cell lines, there was minimal overlap in the induced regions, and neither of the inducible peaks overlapped significantly with TNF inducible peaks (Figure 5A-B). Thus, although both TNF and IFNγ lead to a parallel transition to the dedifferentiated phenotype defined by similar

gene programs, their effects on the chromatin landscape were stimulus-specific. Notably, the undifferentiated cell lines had minimal chromatin remodeling in response to TNF, despite the observed changes in gene expression. In addition, when exposed to continuous IFNγ, these lines had comparable levels of remodeling to that of the baseline differentiated cell lines although they do not undergo further phenotypic dedifferentiation. As the majority of the two groups' IFNγ-induced peaks did not overlap (Figure 5B), the overall response to IFNγ seems to depend on the cell line's baseline epigenomic state.

In order to dissect out peaks that may be attributable to the differences in phenotypic plasticity, all the peaks that were significantly induced from baseline by either IFNγ or TNF were used to perform K-means clustering (Figure 5C). Despite the evidence of cell line heterogeneity, the top transcription factors whose motifs were enriched in the induced peak regions were common across all three clusters for both cytokines. This suggests that, of all IRF1 or IRF2 binding sites throughout the genome that open in response to IFNγ, certain sites selectively open in undifferentiated cell lines (Figure 5C). Similarly, of all ATF3 or BATF binding sites in the genome, certain sites open only in the cell lines that dedifferentiate in response to TNF (Figure 5C).

Upon IFNγ exposure, most IRF and STAT binding sites become hyperaccessible in baseline differentiated and undifferentiated groups except for STAT6. The binding motifs of STAT6 and AP-2 proteins were enriched in the peaks in dedifferentiating cells only, driven by either cytokine. . Upon TNF exposure, the inducible peaks were highly enriched in IRFs and STATs binding sites only in the dedifferentiating group y (Figure 5D). TNF is known to trigger the MAPK pathways, which lead to transcription factor activity of ATF and AP-1 proteins. Motif enrichment analysis revealed that the TNF stimulus lead to the opening of the binding sites of AP-1 factors (Fosl1, Jun-AP, JunB, AP-1, c-Jun, JunD) following TNF-induced dedifferentiation, with no enrichment of these motifs in the inducible peaks of the undifferentiated cell lines following TNF exposure. On

the contrary, the inducible peaks from all samples exposed to IFNγ, regardless of baseline differentiation state, exhibited enrichment of the AP-1 family protein motifs (Figure 5D). In addition, PRDM1 was another factor whose motif had enrichment only in TNF-induced peaks, while the motif for Oct4:Sox17 was only enriched in IFNγ-induced peaks. Altogether, these data show that the baseline epigenomic state of the melanoma cells is the determinant of the resultant differential chromatin landscape modifications from IFNγ or TNF cytokine exposure.

Inferred regulator activity analysis suggests common regulator activity changes between TNF- and IFNγ-induced dedifferentiation

Given the similar binding motifs within families of transcription factors, such as within several IRFs, the NFκB family proteins, and MAPK-activated transcription factors, we next explored the inferred activity of these candidate immune-signaling transcription factors. Using ARACNe (Algorithm for the Reconstruction of Accurate Cellular Network), which uses mutual information to connect regulators and target genes, we constructed reverse-engineer melanoma-specific, IFNγ-response-specific transcriptional networks. We next employed VIPER (Virtual Inference of Protein Activity by Enriched Regulon) to infer the differential activity of over 9000 regulators in cytokine treated versus baseline cell lines. In both TNF- and IFNγ-exposed cell lines, the regulators TFAP2C (AP-2gamma), SOX9, IRF3, and HMGA1 had high inferred activity only with dedifferentiation, confirming the ATAC-seq data. On the other hand, MITF, beta-catenin, and SOX10 had decreased inferred activity only in the dedifferentiating cell lines. In addition, the transcription factors PRDM1, NFKBIA, RXRB, and POU2F2 had positive change in activity in both groups, albeit having higher activity in the dedifferentiating group (Figure 6A and 5B). In addition, the comparison of this gene expression level-derived inferred activity of regulators between TNF and IFNγ-exposed samples showed strong overlap of inferred activity changes in response to each cytokine (Supplemental Figure 4A-D).

Changes in lipid, ribosomal, mitochondrial, and adhesion processes distinguish the TNF- or IFNγ-induced responses in baseline differentiated versus undifferentiated cell lines

To increase our understanding of this new effect of IFNγ on melanoma cells, we performed analysis of the molecular and cellular changes defining pro-inflammatory cytokine-driven dedifferentiation. We used GSEA-squared analysis on gene expression signatures for differentiated and undifferentiated cell line groups exposed to IFNγ or TNF, and looked for the enrichment of programs and processes of interest. All cell lines upregulated immune and inflammatory programs, but the undifferentiated cell lines did not change phenotype with TNF. The differences in TNF-induced chromatin remodeling observed between differentiated and undifferentiated cell lines was correlated with control of lipid, ribosomal, mitochondrial and adhesion gene programs (Figure 7A). For IFNγ, in both the differentiated and undifferentiated cell lines, immune response gene programs are commonly upregulated, while ribosomal and mitochondrial gene sets were downregulated. Consistent with differentiated and undifferentiated cell lines exhibiting more equal magnitude of IFNγ-induced chromatin accessibility changes, there were also fewer divergent gene set categories between these two groups under IFNγ exposure (Figure 7B).

Enrichment of the IFNγ-induced dedifferentiation signature during anti-PD-1 therapy is associated with response

Dedifferentiation of melanoma has been considered a form of resistance to therapy and associated with worse survival of patients (5, 6, 8, 11, 12). However, because we observed the opposite correlation between high *AXL* to *MITF* ratio in biopsies of patients who were responding to anti-PD-1 therapy, we sought to further investigate whether the full IFNγ-driven dedifferentiation signature correlated with therapeutic response. From the seven signatures (four main signatures, three transitional signatures) spanning the four previously defined melanoma subtypes obtained from a previous study (6), the melanocytic subtype was excluded, and the remaining genes were

filtered for the genes with log2 (fold change) of greater than 1 with IFNγ treatment. These select upregulated genes henceforth comprised our IFNγ-induced dedifferentiation signature and was used to interrogate the CheckMate 038 biopsy cohort (19). Increase in the expression of the signature was found following anti-PD-1 therapy in the patients with objective response (CRPR), with no significant changes from baseline in non-responders (Figure 8A). Therefore, biopsies of patients taken while responding to PD-1 blockade therapy show phenotypic dedifferentiation, while non-responding biopsies did not change their differentiation state.

Baseline dedifferentiation in melanoma associates with response to anti-PD-1 therapy and improves outcomes

Finally, we analyzed if the IFNγ-induced dedifferentiation signature could be a baseline prognostic or predictive marker in the CheckMate 038 biopsy cohort, which is representative of advanced and metastatic melanoma samples, and in the melanoma The Cancer Genome Atlas (TCGA) repository, which is representative mainly of primary melanomas and lymph node metastases. There was a significant spread in the expression of the IFNγ-induced dedifferentiation signature at baseline in the CheckMate 038 biopsy cohort, but separation of these 101 baseline biopsies according to response to therapy showed that the biopsies of patients who went onto respond were more likely to have an increased IFNγ-induced dedifferentiation signature ($p = 0.06$ by Wilcoxon test, Figure 8B). Moreover, the IFNγ-induced dedifferentiation signature also correlated positively with overall survival in the TCGA melanoma dataset. Patients whose melanomas had high or intermediate expression of the IFNγ dedifferentiation signature displaying improved overall survival than those with low expression of the signature (Figure 8C). Finally, we confirmed the importance of the melanocytic differentiation state on patient outcomes by analyzing the 84 baseline biopsies from CheckMate 038 for the effect of the expression level of *MITF* and *MART-1/Melan-A* compared to *AXL* on patients' survival. We divided the data in three groups based on the upper and lower quartile of the log2 FPKM expression of each gene. Patients whose baseline

biopsies had low expression of the melanocytic markers *MITF* (Figure 9A) and *MART-1/Melan-A* (Figure 9B) had improved survival, while the group with high *AXL* expression had improved survival (Figure 9C).

Discussion

Here we report a previously unobserved facet of IFNγ, whereby continuous exposure to IFNγ propels melanoma cells toward an altered phenotype with diminished expression of melanosomal markers and increased expression of neural crest markers. Moreover, we demonstrate that melanoma cells exposed to IFNγ and TNF reach two distinct epigenomic states of dedifferentiation despite displaying similar phenotypic dedifferentiation. IFNγ elicited pronounced remodeling of the chromatin landscape in all tested melanoma cell lines regardless of the baseline differentiation status. We observed a number of regulators that have been implicated in melanocyte differentiation, and it is possible that the change in the activity of these regulators may facilitate the backward trajectory. For one, beta-catenin activity was inferred to be decreased in response to TNF- and IFNγ-induced dedifferentiation based on our VIPER analysis, and Wnt/beta-catenin signaling is known to play a role in human melanocyte development from neural crest cells (26). AP-1 has been linked to dedifferentiation in the setting of TNF-induced dedifferentiation in mouse models (27), and we observed that it was one of the top enriched motifs in the chromatin regions opened in TNF-dedifferentiated cells and also in IFNγ-dedifferentiated cells, albeit to a much lesser degree. On the other hand, our analyses also reveal transcription factors with previously unknown involvement in the phenotypic plasticity of human melanomas.

Contrary to the conventional belief that melanocytic dedifferentiation is a state of therapeutic resistance to targeted therapies and immunotherapies (5, 6, 8, 11, 12, 17), we show that the consequence of this phenotypic plasticity depends on the context of the therapy. While it is a resistance mechanism against adoptive cell transfer using T cells against melanosomal antigens (13, 14), we show that it is a surrogate marker for positive response to immune checkpoint blockade therapy. Tumor infiltration by tumor-specific T cells triggers their T cell receptor (TCR) and downstream IFNγ production upon antigen encounter, which is the mechanistic basis of

responses to anti-PD-1 therapy. One of the advantages of IFNγ signaling in cancer cells is the reactive expression of the PD-1 ligand 1 (PD-L1), which provides a mean for the cancer cells to protect themselves from tumor antigen-specific T cell killing (28). These T cells continue to be present in specific regions of the tumor (29), and their production of IFNγ is a favorable prognostic factor that can be detected by a transcriptome of IFNγ response genes (19-21). Once the negative interaction between PD-1 and PD-L1 is released by checkpoint therapies, the antitumor T cells proliferate and produce increased IFNγ leading to an amplification of the antitumor immune response that mediates the clinical benefits (19, 28, 29). Therefore, our observation that responding melanoma biopsies undergo dedifferentiation is highly concordant with our discovery in cell culture model systems that continuous exposure to IFNγ in differentiated melanomas leads to this phenotypic change. Moreover, both in the biopsies of patients treated with anti-PD-1 and in the TCGA melanoma database we noted that the IFNγ-induced dedifferentiation transcriptional signature was associated with improved outcomes. In both cases, it is likely that the dedifferentiation is an indirect reflection of IFNγ produced by tumor antigen-specific T cells. However, as only melanomas that are originally phenotypically differentiated can undergo dedifferentiation upon chronic IFNγ exposure, in these two series the baseline dedifferentiation group is likely to include both melanomas that were originally dedifferentiated independent of a T cell response, and originally differentiated melanomas that dedifferentiate upon T cell recognition and IFNγ production. This dual mechanism leading to dedifferentiation results in difficulty in interpreting the patient biopsy data.

It has been shown that IFNγ from skin-infiltrating CD8+ cytotoxic T cells can inhibit expression of MITF in normal melanocytes (30), indicating that this phenotypic response to pro-inflammatory cytokines may be conserved from melanocytes to melanomas. Therefore, the ability to change the phenotype upon cytokine exposure may have biological advantages that are independent of the malignant transformation of melanocytes. The specific mechanism of how IFNγ leads to the

loss of MITF and gain of neural crest lineage markers is unknown; nonetheless, this study helps to elucidate the epigenetic landscape that characterizes the new phenotypic endpoint driven by IFNγ and the transcriptional regulators that may be partaking in eliciting this change. In summary, melanoma dedifferentiation can be induced by chronic IFNγ exposure and is associated with improved outcomes in patients with melanoma.

Methods

Patient Biopsy Samples and RNA-Sequencing

Study CheckMate 038 (NCT01621490) was a multi-arm, multi-institutional, prospective study to investigate the effects of nivolumab (3 mg/kg every 2 weeks) single agent, or the combination of nivolumab (1 mg/kg every 3 weeks) plus ipilimumab (3 mg/kg every 3 weeks) given for four doses and followed by nivolumab (3 mg/kg every 2 weeks) single agent (18, 19). Patients were treated until progression or for a maximum of 2 years, or were stopped due to toxicities. Radiographic assessment of response was performed approximately every 8 weeks until progression. Progression was confirmed with a repeat CT scan at least four weeks later. Tumor response for patients was defined by RECIST v1.1. Response to therapy indicates best overall response unless otherwise indicated. All patients underwent a baseline biopsy before commencing therapy (1 to 7 days before the first dose of therapy) and a repeat biopsy, on cycle 1, day 29 (between days 23–29).

Baseline and on-therapy tumor tissue biopsies were stored with RNAlater (Ambion) for subsequent RNA extraction using Qiagen kits. Of 170 patients, 101 had enough RNA for RNAseq (Figure 1). RNA-seq library was prepared using Illumina Truseq Stranded mRNA kit. Sequencing was done on an Illumina HiSeq sequencer using paired end sequencing of 50 bp for each mate pair. RNA-seq reads were mapped using HISAT2 version 2.0.4 (31) and aligned to the hg19 genome using default parameters. Reads were quantified by HTSeq version 0.6.1 (32) with the intersection-non-empty mode and counting ambiguous reads if fully overlapping. Raw counts were then normalized to fragments per kilobase of exon per million fragments mapped (FPKM) expression values.

Cell Culture and *In Vitro* Cytokine Stimulation

Human melanoma cell lines (M series) were established from patient's biopsies under UCLA IRB approval #11–003254 and human melanoma cell line 3998mel was provided by Alena Gros (33). Cells were cultured in RPMI 1640 with L-glutamine (Mediatech), 10% fetal bovine serum (Omega Scientific), and 1% penicillin-streptomycin (Omega Scientific) and were incubated in a water-saturated incubator at 37°C with 5% CO2. Cell lines were periodically authenticated to their early passages using GenePrint® 10 System (Promega). Human recombinant IFNγ (Milipore Sigma) and human recombinant TNF (Peprotech) were each reconstituted in molecular grade water to 0.5 mg/ml and diluted in 0.1% BSA in PBS to 0.1 mg/ml before applying to cell culture media. The cytokines were stored in -80°C. For *in vitro* long-term IFNγ experiments, cell lines were expanded and seeded onto 10cm tissue culture-treated plates at 70% confluency. After 24 hours to allow the cells to adhere to the plates, new cell culture media containing 500 U/mL of human recombinant IFNγ protein were added. The cells were replenished with IFNγ-containing media every 2-3 days. Cells were seeded into multiple tissue culture plates and treated concurrently, so that a plate of cells could be harvested to perform flow cytometry each week without perturbing the rest of the cells and their ongoing exposure to interferon-gamma. For *in vitro* TNF experiments, the dose and time duration of exposure were kept same as the previously reported study to use as positive control (13). Therefore, media containing 1000 U/mL of human recombinant TNF were added to plates of seeded cells and kept unperturbed for three days until the cells were harvested for downstream experiments.

Flow Cytometry

Cells were trypsinized, washed with PBS, and pelleted by centrifuging at 4°C for 5 minutes at 1500 RPM. All subsequent steps were performed with the cells on ice. Zombie Violet Fixable Viability Kit (BioLegend) was used per manufacturer's instructions. Next, cells were incubated in fetal bovine serum for 10 minutes to block unspecific binding. Cells were then incubated with anti-NGFR (PE) antibody (BioLegend) in PBS for 20 minutes. Following a wash, Cytofix/Cytoperm

Fixation and Permeabilization Solution (BD Biosciences) was used per manufacturer's instructions to allow for the subsequent intracellular MART-1 staining. All subsequent wash steps were performed using 1X Perm/Wash Buffer (BD Biosciences). Cells were incubated with anti-MART-1 (Alexa Fluor 647) antibody (Santa Cruz Biotechnology) for 20 minutes and washed. OneComp eBeads compensation beads (ThermoFisher) were used for compensation. The samples were run on the FACSCelesta Flow Cytometer (BD Biosciences), and the data were analyzed using the FlowJo software (TreeStar, Inc.).

RNA-Sequencing

RNA extraction was performed using the AllPrep DNA/RNA Mini Kit (Qiagen). Library preparation was performed by the Technology Center for Genomics & Bioinformatics (TCGB) at UCLA. RNA was sequenced on the HiSeq 3000 Sequencing System (Illumina) for a single-end 50 base run. Data quality was checked on Sequencing Analysis Viewer software (Illumina), and demultiplexing was performed using the bcl2fastq2 Conversion Software v2.17 (Illumina). Raw FASTQ data files were aligned to the hg19 genome using HISAT2 v2.0.4 with default parameters and counted using HTSeq v0.6.1. The raw counts were normalized to fragments per kilobase of exon per million fragments mapped (FPKM). DESeq2 was used to perform differential gene expression analysis. The raw RNA data is deposited in the Gene Expression Omnibus (GEO) database under accession number GSE152755.

Omni-ATAC Library Preparation and Sequencing

Cultured cells were harvested by trypsinization and were checked for viability of greater than 90%. After the cells were counted, 50,000 cells were resuspended in 1 ml of cold ATAC-seq resuspension buffer (RSB; 10 mM Tris-HCl pH 7.4, 10 mM NaCl, and 3 mM MgCl2 in water). Cells were centrifuged at 500 RCF for 5 minutes at 4°C in a fixed-angle centrifuge. Supernatant was carefully removed using two-step pipetting to avoid the cell pellet. Cell pellets were then

resuspended in 50 µl of ATAC-seq RSB containing 0.1% NP40, 0.1% Tween-20, and 0.01% digitonin by pipetting up and down three times. This cell lysis reaction was incubated on ice for 3-5 minutes, with the lysis time optimized for each sample. After lysis, 1 ml of ATAC-seq RSB containing 0.1% Tween-20 was added, and the tubes were inverted to mix. Nuclei were then centrifuged for 10 minutes at 500 RCF at 4°C in a fixed-angle centrifuge. Supernatant was carefully removed with two-step pipetting, and the nuclei were resuspended in 50 µl of transposition mix, which consisted of 25 µl of 2x TD buffer, 2.5 µl transposase (Illumina Nextera DNA Library Prep Kit), with 16.5 µl PBS, 0.5 µl 1% digitonin, 0.5 µl 10% Tween-20, and 5 µl water. Transposition reactions were incubated at 37°C for 1 hour in a thermomixer with shaking at 800 RPM. Reactions were cleaned up with Zymo DNA Clean and Concentrator columns and eluted in 10ul of nuclease-free water.

Following purification, the transposed DNA fragments were amplified using 1x NEBnext PCR Master Mix (New England BioLabs) and 1.25 µM of the Ad1_noMX primer and of the indexing primer (34) in nuclease-free water for a 50 µl reaction, with the following PCR conditions: 72°C for 5 minutes; 98°C for 30 seconds; and thermocycling at 98°C for 10 seconds, 63°C for 30 seconds and 72°C for 1 minute, for five cycles. To reduce GC content and size bias, qPCR was performed to determine the appropriate amount of amplification before saturation. To do this, 5 µL aliquot of the PCR reaction was added to 10 µl of the above PCR cocktail with the final concentration of 0.6x of SYBR Green (Thermo Fisher). The qPCR cycle was run at 98°C for 30 seconds followed by 20 cycles of 98°C for 10 seconds, 63°C for 30 seconds, and 72°C for 1 minute to determine the additional number of cycles needed for the remaining 45 µL reaction. The libraries were purified using a Qiagen MinElute PCR Purification Kit. All libraries met the target concentration of 20 µl at 4 nM, determined by the Qubit Fluorometric Quantitation (Thermo Fisher). Sequencing was performed on the NextSeq 500 (Illumina) for a paired-end 75 base run, and at

least 50 million paired reads were obtained for each sample. The raw ATAC data is deposited in the Gene Expression Omnibus (GEO) database under accession number GSE154483.

Omni-ATAC Data Processing

The raw FASTQ files were processed using the published ENCODE ATAC-seq Pipeline (https://github.com/kundajelab/atac_dnase_pipelines). The reads were trimmed and aligned to hg38 using bowtie2. Picard was used to de-duplicate reads, which were then filtered for high quality, paired reads using samtools. All peak calling was performed using macs2. The optimal Irreproducible Discovery Rate (IDR) thresholded peak output was used for all downstream analyses, with a threshold p-value of 0.05. Other ENCODE3 parameters were enforced with the flag --encode3. Reads that mapped to mitochondrial genes or blacklisted regions, as defined by the ENCODE pipeline, were removed. The peak files were merged using bedtools merge to create a consensus set of peaks across all samples, and the number of reads in each peak was determined using bedtools multicov (35). DESeq2 with default parameters was used to normalize read counts (36) and to determine the the hyperaccessible and hypoaccessible peaks following cytokine exposure. Peaks were called as hyper- or hypo-accessible using abs (log2 fold change)>0.5 and adjusted $p<0.05$.

PCA/PLSR and projections

Log2 transformed fragments per kilobase per million (FPKM) of coding genes was used to perform unsupervised principal component analysis (PCA). This method uncovers latent components which are linear combinations of the features that most strongly vary across the datasets. PCA was performed centered and unscaled using the *prcomp* function in R. Projections onto PCA frameworks were done using custom script by multiplication of the original projected sample scores by the PCA rotation matrix. PCA of ATACseq data was performed centered and unscaled using normalized counts of the union of all significantly induced peaks. Partial Least Squares

Regression (PLSR) is a supervised version of PCA that seeks to find the latent vectors that maximize the covariance of the input variables (e.g. gene expression) and the response (e.g. phenotypes). Varimax rotation of the PLSR loadings ($PLSR_v$) was performed on 2 components, without Kaiser normalization and using the R package *varimax*, in order to simplify the structure of the loading matrix.

Mutation Analysis

The patient-derived human melanoma cell lines were sequenced and characterized for their mutational status as previously described (7, 37, 38).

Gene Set Enrichment Analysis and Gene Ontology

Gene Set Enrichment Analysis (GSEA) (39) and GSEA-squared was done on pre-ranked lists of genes using the MSigDB C5 gene sets and Kolmogorov-Smirnov (KS) statistics. GSEA-squared was performed as previously described (25). Briefly, all individual words in the genesets were collected and their frequencies were tabulated. Words with frequencies <5 or >500 were excluded, and all gene sets were then ranked by their NES value. Keywords and their categories were further assigned by manual curation of the top of the ranked list of words.

Rank Rank Hypergeometric Overlap (RRHO)

Rank Rank Hypergeometric Overlap was performed for gene expression data by taking the rank of varimax-rotated PLSR loadings, and calculating the hypergeometric p-values of the TNF-d0 versus IFNγ-d0 ranked lists using the online tool and the R package RRHO. RRHO for genesets was performed after running GSEA on ranked gene lists, and ranking gene sets by their Normalized Enrichment Score. Step size 100 was used for genes and gene sets (24).

Motif Enrichment Analysis

Differential peak analysis was first conducted using DESeq2 on normalized ATACseq counts. Starting from the full consensus peak set, samples were divided into baseline differentiated and baseline undifferentiated groups, and hypo- and hyper-accessible peaks were called separately for TNF vs d0, and IFNγ vs d0, at adjusted p-value < 0.05 and log2 fold-change >2, without independent filtering or Cook's cutoff. Motif analysis was done on each of these peak sets using HOMER against a whole genome background and searching for motifs within +/-200bp from the peak center. Raw -ln(p-values) were plotted for TNF-induced vs IFNγ-induced hyper accessible motifs. Overlap of significantly differential peaks was calculated and plotted as Venn diagrams using the R package *Vennerable*.

ARACNe and VIPER Analysis

ARACNe (40) network connections were created using all genes, and then the network nodes were restricted to transcription factors (TFs) by combining all TF gene sets in the GO gene ontology. A single network was built using melanoma RNAseq samples from the M-series cohort (19). VIPER analysis (41) was performed using the R *msviper* function from the package viper, with a minimum network size of 10.

TCGA Survival Analyses

Patient samples from the TCGA were divided into groups of low (lower quartile), median (interquartile range) and high (upper quartile) based on the expression of IFNγ-induced dedifferentiation signature. Patient clinical annotations were obtained from the TCGA skin cutaneous melanoma publication (PMID: 26091043) and overall survival was determined using the 'curated TCGA days to death or last fu'.

Statistics

Analysis of IFNγ-induced dedifferentiation signature in biopsies from patients in the CheckMate 038 was performed by Wilcoxon test. TCGA survival analysis was performed using the Kaplan-Meier method using the R survival package and plots were generated using the ggsurv R package. Statistical significance was determined using the log-rank test.

Study Approvals

The CheckMate 038 (NCT01621490) clinical trial protocol and its amendments were approved by the relevant local institutional review boards where patients were enrolled, and the study was conducted in accordance with the Declaration of Helsinki and the International Conference on Harmonization Guidelines for Good Clinical Practice. All patients signed written informed consent prior to having any study procedures performed.

Author Contributions

A.R. conceived and supervised the project. Y.J.K. and A.R. designed the experiments and interpreted the results. Y.J.K conducted the research and analyzed the data. K.M.S. and Y.J.K. decided on the bioinformatic approaches and analyses. K.M.S. performed the ATAC-seq and RNA-seq bioinformatic analyses. J.T. performed RNA-seq processing and bioinformatic analyses. J.T., G.A-R., E.M., and C.S.G. performed analysis of the clinical biopsy cohort. D.Y.T., A.S.C., K.L., C.S., D.E.S., P.O.S., A.H., T.G.G., and C.P-S. contributed technical and scientific expertise for experimental design or analysis. Y.J.K., K.M.S., and A.R. wrote the manuscript with input from the co-authors. All authors reviewed and approved the manuscript.

Acknowledgements

We would like to thank Stephen T. Smale at UCLA for kindly sharing his expertise and providing guidance. We would like to thank Hong Zhang at the Technology Center for Genomics and Bioinformatics Core Facility at UCLA for her helpful discussions on ATAC-sequencing. We would also like to thank Alena Gros for kindly sharing the cell line 3998mel. Y.J.K. was supported by the NIH Ruth L. Kirschstein Institutional National Research Service Award F30 CA243248 and the NIH NIGMS training grant T32-GM008042. K.M.S. was supported by the NIH NIGMS training grant T32-GM008042 and T32-GM008185. J.T. was supported by the NIH T32-CA009120. G.A-R. was supported by the Isabel & Harvey Kibel Fellowship award and the Alan Ghitis Fellowship Award for Melanoma Research. D.Y.T. was supported by a Young Investigator Award from ASCO, a grant from the Spanish Society of Medical Oncology for Translational Research in Reference Centers and the V Foundation-Gil Nickel Family Endowed Fellowship in Melanoma Research. A.H. was funded by NIH grant R01AI132835. C.P.S. is a recipient of a Parker Senior Fellow Award from the Parker Institute for Cancer Immunotherapy. T.G.G. and A.R. were funded by NIH grant P01 CA244118. A.R. was funded by the Parker Institute for Cancer Immunotherapy, NIH grants R35 CA197633 and P30 CA016042, the Ressler Family Fund, and the Ken and Donna Schultz Fund.

References

1. Yoshida H, Kunisada T, Kusakabe M, Nishikawa S, and Nishikawa SI. Distinct stages of melanocyte differentiation revealed by anlaysis of nonuniform pigmentation patterns. *Development.* 1996;122(4):1207-14.
2. Restivo G, Diener J, Cheng PF, Kiowski G, Bonalli M, Biedermann T, et al. low neurotrophin receptor CD271 regulates phenotype switching in melanoma. *Nat Commun.* 2017;8(1):1988.
3. Hoek KS, Eichhoff OM, Schlegel NC, Dobbeling U, Kobert N, Schaerer L, et al. In vivo switching of human melanoma cells between proliferative and invasive states. *Cancer Res.* 2008;68(3):650-6.
4. Hoek KS, Schlegel NC, Eichhoff OM, Widmer DS, Praetorius C, Einarsson SO, et al. Novel MITF targets identified using a two-step DNA microarray strategy. *Pigment Cell Melanoma Res.* 2008;21(6):665-76.
5. Tirosh I, Izar B, Prakadan SM, Wadsworth MH, 2nd, Treacy D, Trombetta JJ, et al. Dissecting the multicellular ecosystem of metastatic melanoma by single-cell RNA-seq. *Science.* 2016;352(6282):189-96.
6. Tsoi J, Robert L, Paraiso K, Galvan C, Sheu K, Lay J, et al. Multi-stage differentiation defines melanoma subtypes with differential vulnerability to drug-induced iron-dependent oxidative stress. *Cancer Cell.* 2018;(in press).
7. Nazarian R, Shi H, Wang Q, Kong X, Koya RC, Lee H, et al. Melanomas acquire resistance to B-RAF(V600E) inhibition by RTK or N-RAS upregulation. *Nature.* 2010;468(7326):973-7.
8. Muller J, Krijgsman O, Tsoi J, Robert L, Hugo W, Song C, et al. Low MITF/AXL ratio predicts early resistance to multiple targeted drugs in melanoma. *Nat Commun.* 2014;5:5712.
9. Tachibana M, Takeda K, Nobukuni Y, Urabe K, Long JE, Meyers KA, et al. Ectopic expression of MITF, a gene for Waardenburg syndrome type 2, converts fibroblasts to cells with melanocyte characteristics. *Nat Genet.* 1996;14(1):50-4.
10. Opdecamp K, Nakayama A, Nguyen MT, Hodgkinson CA, Pavan WJ, and Arnheiter H. Melanocyte development in vivo and in neural crest cell cultures: crucial dependence on the Mitf basic-helix-loop-helix-zipper transcription factor. *Development.* 1997;124(12):2377-86.
11. Konieczkowski DJ, Johannessen CM, Abudayyeh O, Kim JW, Cooper ZA, Piris A, et al. A melanoma cell state distinction influences sensitivity to MAPK pathway inhibitors. *Cancer Discov.* 2014;4(7):816-27.
12. Rambow F, Rogiers A, Marin-Bejar O, Aibar S, Femel J, Dewaele M, et al. Toward Minimal Residual Disease-Directed Therapy in Melanoma. *Cell.* 2018;174(4):843-55 e19.
13. Landsberg J, Kohlmeyer J, Renn M, Bald T, Rogava M, Cron M, et al. Melanomas resist T-cell therapy through inflammation-induced reversible dedifferentiation. *Nature.* 2012;490(7420):412-6.
14. Mehta A, Kim YJ, Robert L, Tsoi J, Comin-Anduix B, Berent-Maoz B, et al. Immunotherapy Resistance by Inflammation-Induced Dedifferentiation. *Cancer Discov.* 2018;8(8):935-43.

15. Holzel M, and Tuting T. Inflammation-Induced Plasticity in Melanoma Therapy and Metastasis. *Trends Immunol.* 2016;37(6):364-74.
16. Falletta P, Sanchez-Del-Campo L, Chauhan J, Effern M, Kenyon A, Kershaw CJ, et al. Translation reprogramming is an evolutionarily conserved driver of phenotypic plasticity and therapeutic resistance in melanoma. *Genes Dev.* 2017;31(1):18-33.
17. Massi D, Mihic-Probst D, Schadendorf D, Dummer R, and Mandala M. Dedifferentiated melanomas: Morpho-phenotypic profile, genetic reprogramming and clinical implications. *Cancer Treat Rev.* 2020;88:102060.
18. Riaz N, Havel JJ, Makarov V, Desrichard A, Urba WJ, Sims JS, et al. Tumor and Microenvironment Evolution during Immunotherapy with Nivolumab. *Cell.* 2017;171(4):934-49 e16.
19. Grasso CS, Tsoi J, M. O, Abril-Rodriguez G, Ross-Macdonald P, Wind-Rotolo M, et al. Conserved interferon-ɣ signaling drives clinical response to immune checkpoint blockade therapy in melanoma. *Cancer Cell.* 2020;(in press).
20. Ayers M, Lunceford J, Nebozhyn M, Murphy E, Loboda A, Kaufman DR, et al. IFN-gamma-related mRNA profile predicts clinical response to PD-1 blockade. *J Clin Invest.* 2017;127(8):2930-40.
21. Cristescu R, Mogg R, Ayers M, Albright A, Murphy E, Yearley J, et al. Pan-tumor genomic biomarkers for PD-1 checkpoint blockade-based immunotherapy. *Science.* 2018;362(6411).
22. Zaretsky JM, Garcia-Diaz A, Shin DS, Escuin-Ordinas H, Hugo W, Hu-Lieskovan S, et al. Mutations Associated with Acquired Resistance to PD-1 Blockade in Melanoma. *N Engl J Med.* 2016;375(9):819-29.
23. Shin DS, Zaretsky JM, Escuin-Ordinas H, Garcia-Diaz A, Hu-Lieskovan S, Kalbasi A, et al. Primary Resistance to PD-1 Blockade Mediated by JAK1/2 Mutations. *Cancer Discov.* 2017;7(2):188-201.
24. Plaisier SB, Taschereau R, Wong JA, and Graeber TG. Rank-rank hypergeometric overlap: identification of statistically significant overlap between gene-expression signatures. *Nucleic acids research.* 2010;38(17):e169.
25. Balanis NG, Sheu KM, Esedebe FN, Patel SJ, Smith BA, Park JW, et al. Pan-cancer Convergence to a Small-Cell Neuroendocrine Phenotype that Shares Susceptibilities with Hematological Malignancies. *Cancer Cell.* 2019;36(1):17-34 e7.
26. Bellei B, Pitisci A, Catricala C, Larue L, and Picardo M. Wnt/beta-catenin signaling is stimulated by alpha-melanocyte-stimulating hormone in melanoma and melanocyte cells: implication in cell differentiation. *Pigment Cell Melanoma Res.* 2011;24(2):309-25.
27. Riesenberg S, Groetchen A, Siddaway R, Bald T, Reinhardt J, Smorra D, et al. MITF and c-Jun antagonism interconnects melanoma dedifferentiation with pro-inflammatory cytokine responsiveness and myeloid cell recruitment. *Nat Commun.* 2015;6:8755.
28. Ribas A, and Wolchok JD. Cancer immunotherapy using checkpoint blockade. *Science.* 2018;359(6382):1350-5.
29. Tumeh PC, Harview CL, Yearley JH, Shintaku IP, Taylor EJ, Robert L, et al. PD-1 blockade induces responses by inhibiting adaptive immune resistance. *Nature.* 2014;515(7528):568-71.
30. Yang L, Wei Y, Sun Y, Shi W, Yang J, Zhu L, et al. Interferon-gamma Inhibits Melanogenesis and Induces Apoptosis in Melanocytes: A Pivotal Role of CD8+ Cytotoxic T Lymphocytes in Vitiligo. *Acta Derm Venereol.* 2015;95(6):664-70.

31. Kim D, Paggi JM, Park C, Bennett C, and Salzberg SL. Graph-based genome alignment and genotyping with HISAT2 and HISAT-genotype. *Nat Biotechnol.* 2019;37(8):907-15.
32. Anders S, Pyl PT, and Huber W. HTSeq--a Python framework to work with high-throughput sequencing data. *Bioinformatics.* 2015;31(2):166-9.
33. Gros A, Parkhurst MR, Tran E, Pasetto A, Robbins PF, Ilyas S, et al. Prospective identification of neoantigen-specific lymphocytes in the peripheral blood of melanoma patients. *Nat Med.* 2016;22(4):433-8.
34. Buenrostro JD, Giresi PG, Zaba LC, Chang HY, and Greenleaf WJ. Transposition of native chromatin for fast and sensitive epigenomic profiling of open chromatin, DNA-binding proteins and nucleosome position. *Nat Methods.* 2013;10(12):1213-8.
35. Quinlan AR, and Hall IM. BEDTools: a flexible suite of utilities for comparing genomic features. *Bioinformatics.* 2010;26(6):841-2.
36. Love MI, Huber W, and Anders S. Moderated estimation of fold change and dispersion for RNA-seq data with DESeq2. *Genome Biol.* 2014;15(12):550.
37. Atefi M, Avramis E, Lassen A, Wong DJ, Robert L, Foulad D, et al. Effects of MAPK and PI3K Pathways on PD-L1 Expression in Melanoma. *Clin Cancer Res.* 2014;20(13):3446-57.
38. Wong DJ, Robert L, Atefi MS, Lassen A, Avarappatt G, Cerniglia M, et al. Antitumor activity of the ERK inhibitor SCH722984 against BRAF mutant, NRAS mutant and wild-type melanoma. *Mol Cancer.* 2014;13:194.
39. Subramanian A, Tamayo P, Mootha VK, Mukherjee S, Ebert BL, Gillette MA, et al. Gene set enrichment analysis: a knowledge-based approach for interpreting genome-wide expression profiles. *Proc Natl Acad Sci U S A.* 2005;102(43):15545-50.
40. Lachmann A, Giorgi FM, Lopez G, and Califano A. ARACNe-AP: gene network reverse engineering through adaptive partitioning inference of mutual information. *Bioinformatics.* 2016;32(14):2233-5.
41. Alvarez MJ, Shen Y, Giorgi FM, Lachmann A, Ding BB, Ye BH, et al. Functional characterization of somatic mutations in cancer using network-based inference of protein activity. *Nat Genet.* 2016;48(8):838-47.

Figures Legends

Figure 1. Human melanoma dedifferentiation is associated with response to anti PD-1 therapy. A) *MITF,* B) *MLANA,* and C) *AXL* gene expression levels in pre- and post-treatment biopsies from patients with progressive disease (PD), stable disease (SD), and complete or partial response (CRPR).

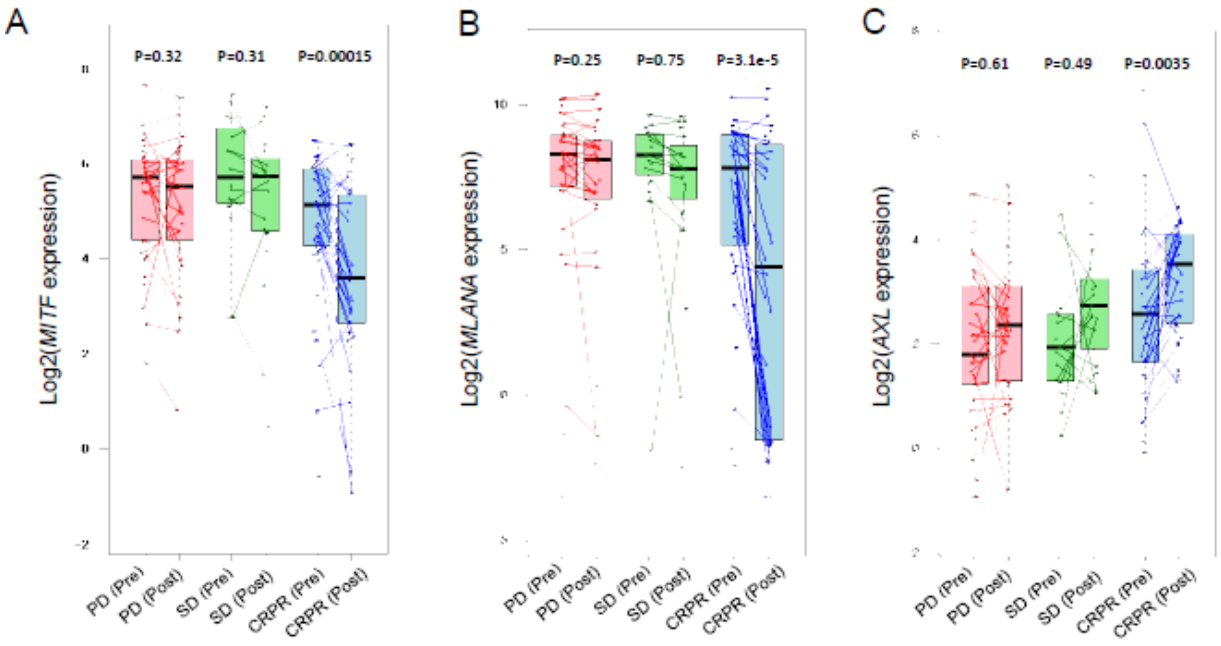

Figure 2. Human melanoma dedifferentiation is induced by exposure to IFNγ. A) Flow cytometry data for MART-1 and NGFR on M262 (baseline differentiated) and M370 (baseline undifferentiated) in response to TNF or IFNγ. B) Projection of cytokine-treated cell lines onto melanoma M series differentiation PCA (Tsoi et al.). Diff = baseline differentiated, undiff = baseline undifferentiated. C) Expression of melanoma differentiation genes for 0hr, IFNγ, and TNF across cell lines (U= Undifferentiated, U-NC= Undifferentiated-Neural crest-like, NC= Neural crest-like, NC-T= Neural crest-like-Transitory, T= Transitory, T-M= Transitory-Melanocytic, M= Melanocytic). Colors represent z scores. D) Common melanoma mutations across cell lines studies. Nonsense or missense JAK/STAT mutations were not observed.

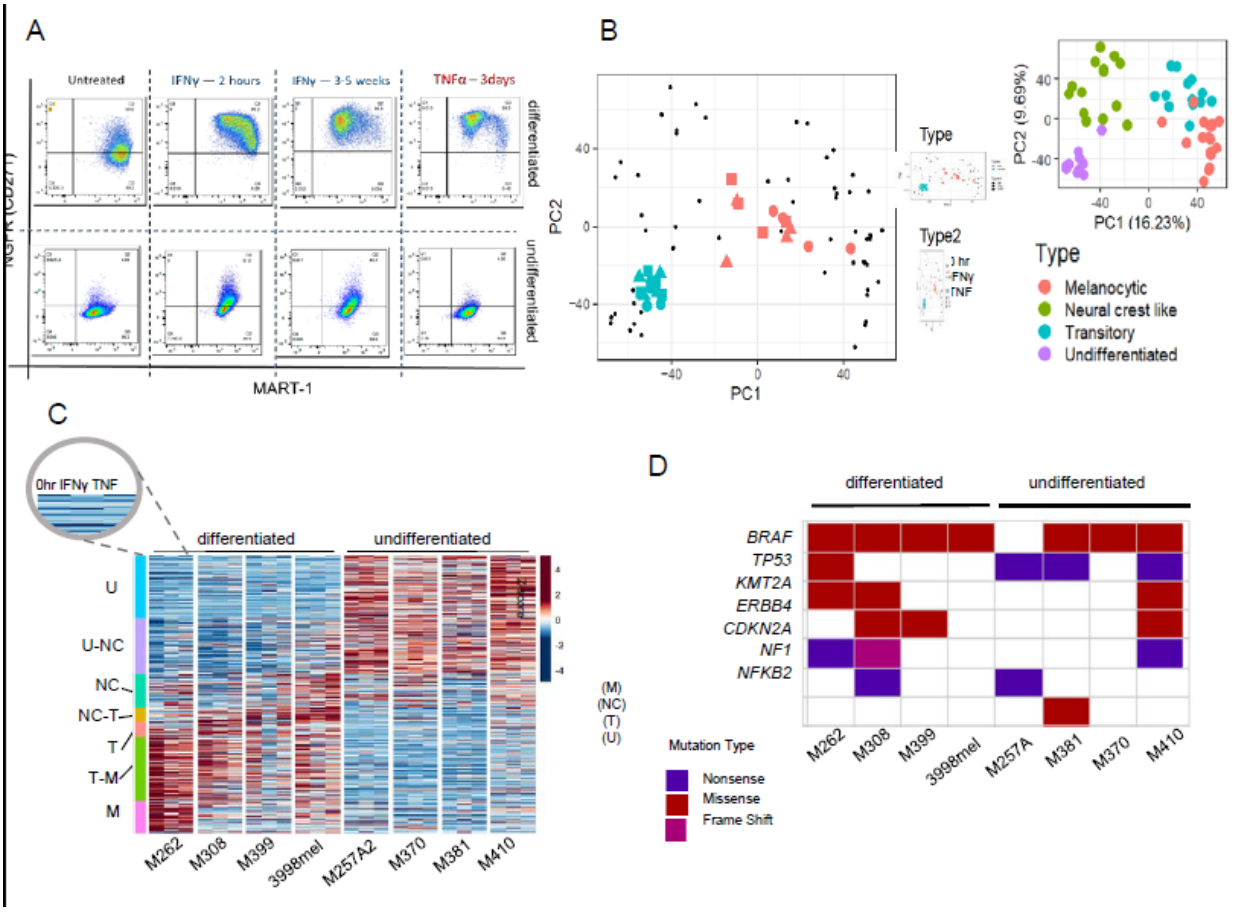

Figure 3. IFNγ and TNF stimulation induce common genes across cell lines to generate comparable MART-1-low/NGFR-high dedifferentiation states. A) Varimax-rotated PLSR on IFNγ-exposed compared to 0-hour (untreated) samples. B) (left) Genes contributing to common IFNγ response across samples. (right) K-means clustering of top 300 gene loadings. Left column is untreated and right column is post-IFNγ exposure for each cell line. C) Varimax-rotated PLSR on TNF compared to untreated samples. D) (left) Genes contributing to TNF response across samples. (right) K-means clustering of top 300 gene loadings. Left column is untreated and right column is post-TNF exposure for each cell line. E) Overlap of IFNγ and TNF induced gene expression by ranked loadings. F) Concordant gene ontology term overlap (normalized enrichment scores) between IFNγ and TNF-induced gene expression. G-H) Enrichment of gene sets involving pigmentation, mitosis, transcription, interferon signaling, and cytokines following IFNγ or TNF exposure.

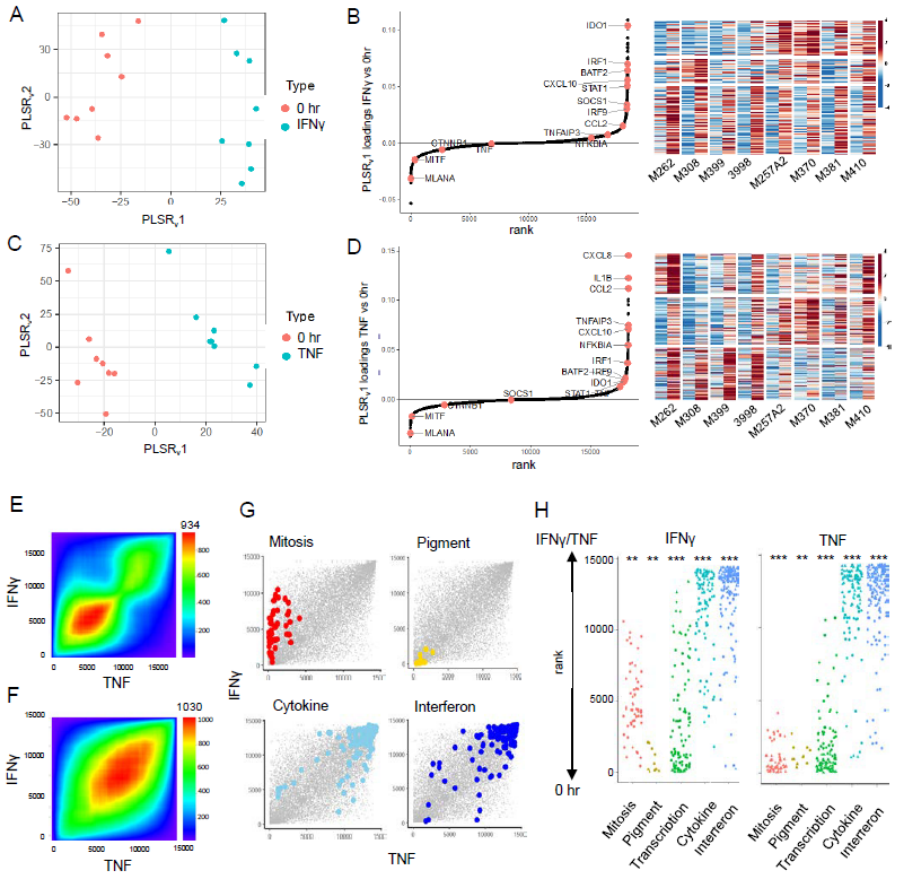

Figure 4. IFNγ compared to TNF alter the chromatin landscape in a stimulus-specific manner. A) Examples of hyper-accessible peaks upon cytokine stimulation. B) Total number of hyper and hypo-accessible peaks called for each listed comparison (U = Undifferentiated at baseline, D = Differentiated at baseline). C) PCA of peaks differentially hyper-accessible from baseline after cytokine treatment. D) K-means clustered heatmap of induced ATACseq peaks across any stimulation condition for differentiated and undifferentiated melanomas (sub-columns are in the order 0 hour, IFNγ, and TNF for each cell line). E) Motif enrichment of IFNγ compared to TNF induced genes. F) Top divergent gene ontology terms of nearby genes for IFNγ compared to TNF-specific peaks.

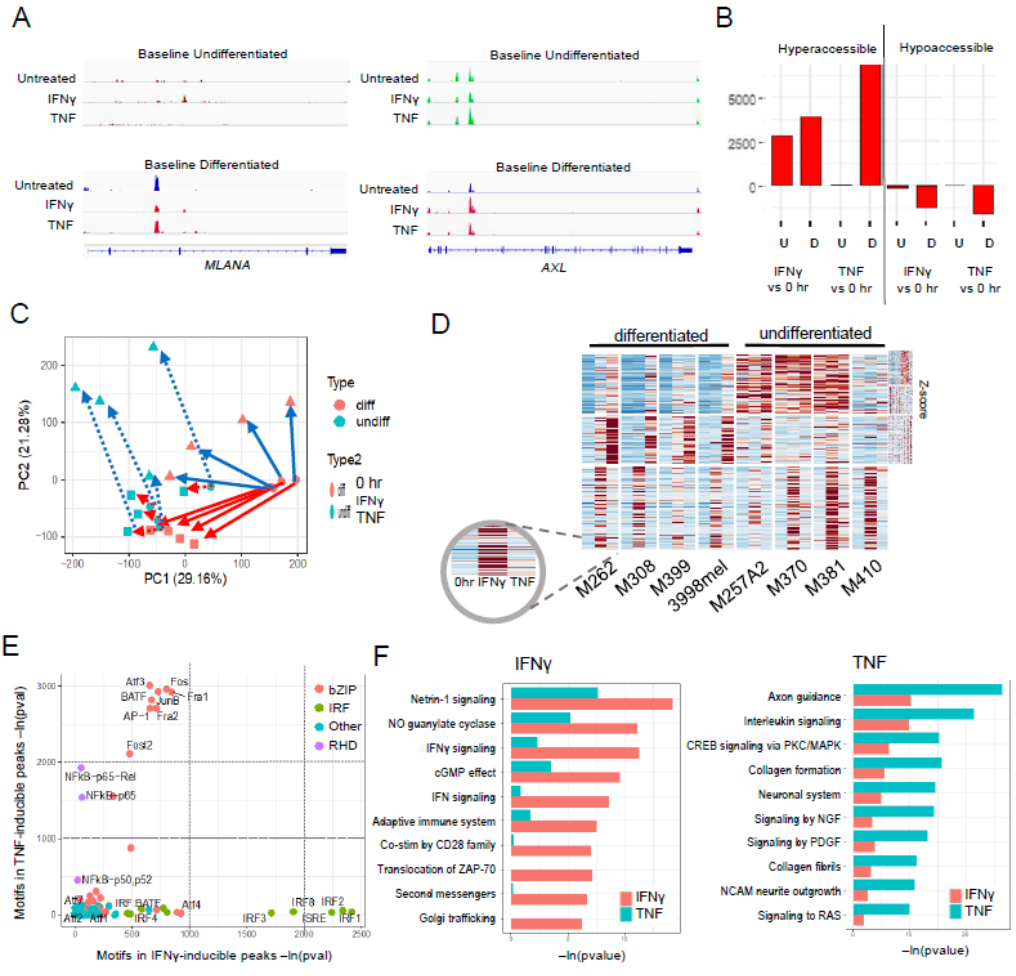

Figure 5. The basal chromatin landscapes of differentiated and undifferentiated lines result in distinct epigenomic responses upon cytokine stimulation. A) Overlap of induced IFNγ and TNF ATACseq peaks. B) Overlap of peaks separated by cell line baseline state (Diff = baseline differentiated, Undiff = baseline undifferentiated). C) Heatmap of differentially IFNγ inducible peaks for baseline differentiated and undifferentiated lines, with top motif of each cluster listed (sub-columns are in the order 0 hour, IFNγ, and TNF for each cell line). D) Heatmap of differentially TNF inducible peaks for baseline differentiated and undifferentiated lines, with top motif of each cluster listed. D) Motif enrichment of IFNγ compared to TNF inducible peaks for baseline differentiated and undifferentiated lines separately (U= baseline undifferentiated, D = baseline differentiated). Colors represent q values.

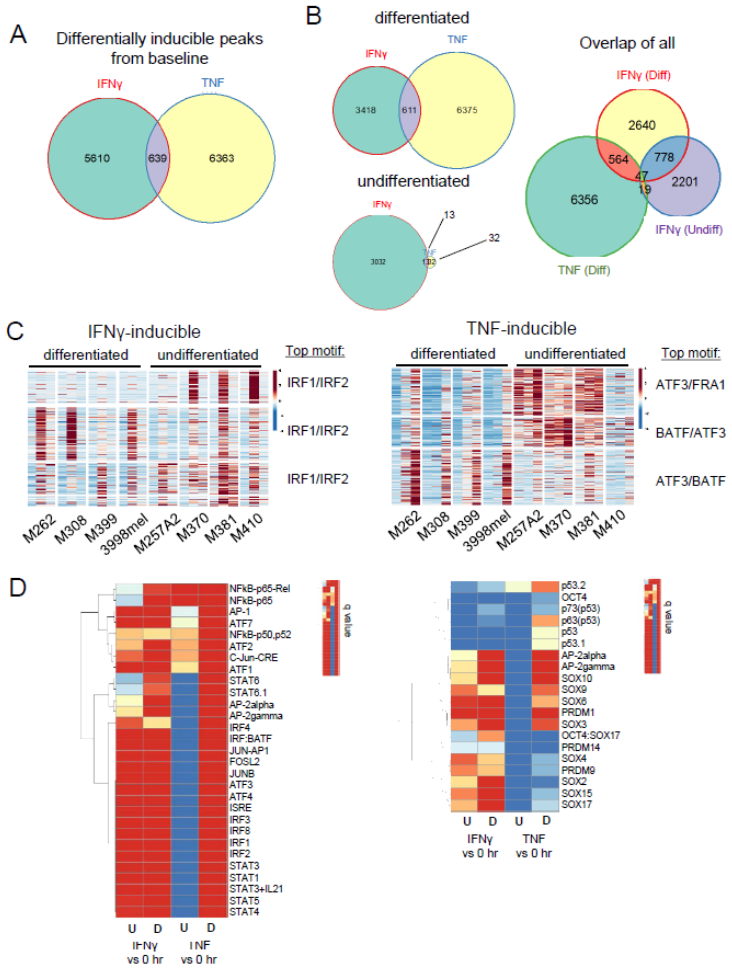

Figure 6. Differentiated and undifferentiated lines respond to cytokine stimulation with differences in inferred activity of both signal-dependent and lineage determining transcription factors. A-B) VIPER analysis showing inferred TF activity for baseline differentiated versus undifferentiated lines following (A) TNF or (B) IFNγ exposure. Regulators such as PRDM1, HMGA1, SOX9 have high inferred activity only in the baseline differentiated group.

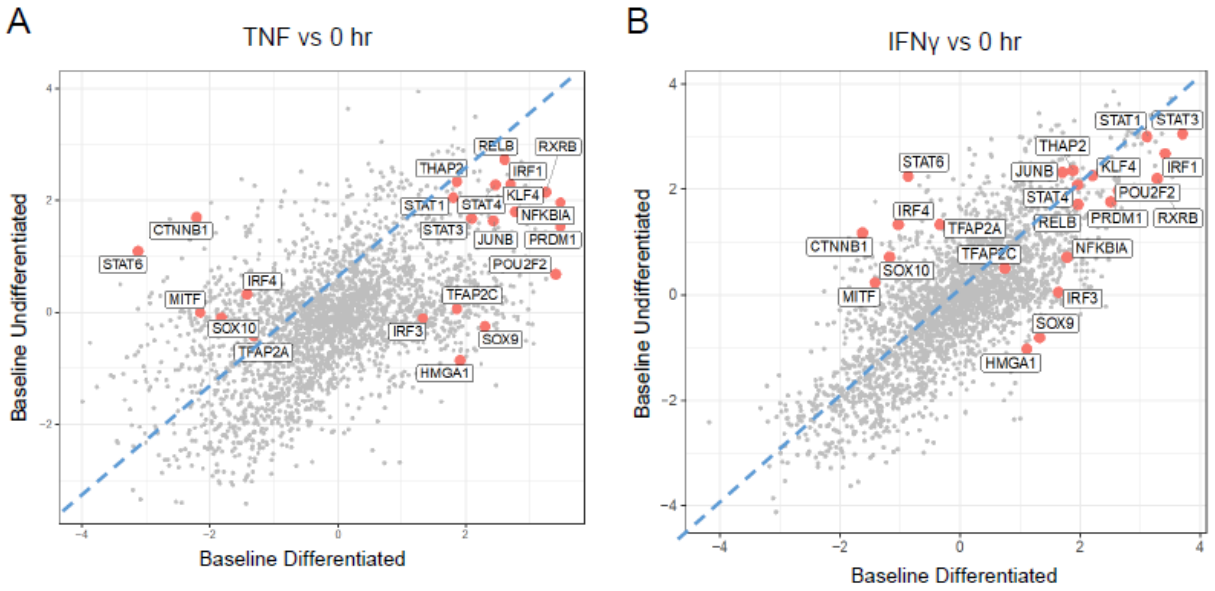

Figure 7. Gene expression differences between differentiated and undifferentiated lines may be attributed to lipid, ribosomal, mitochondrial, and adhesion processes. A-B) Enrichment of gene set groups (C5: GO gene sets) based on ranked lists of differentially expressed genes, for TNF or IFNγ.

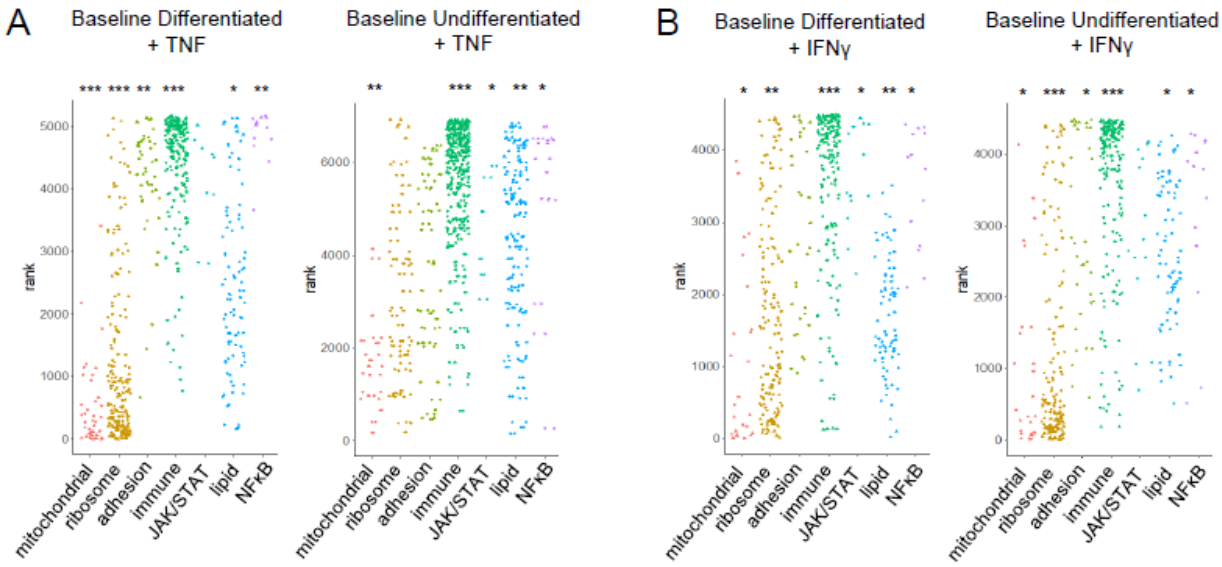

Figure 8. The enrichment of IFNγ-induced dedifferentiation gene signatures in melanomas correlate with response to anti-PD-1 and better overall survival. A) Enrichment of the dedifferentiation signature in the paired pre- and post-treatment biopsies (n=68) of responders and non-responders from the Checkmate 038 biopsy cohort. B) Enrichment of the dedifferentiation signature in the baseline biopsies of the Checkmate 038 biopsy cohort, including the paired and unpaired biopsies (n=101), from responders and non-responders. C) Correlation of baseline enrichment of the dedifferentiation signature with overall survival in the TCGA melanoma dataset.

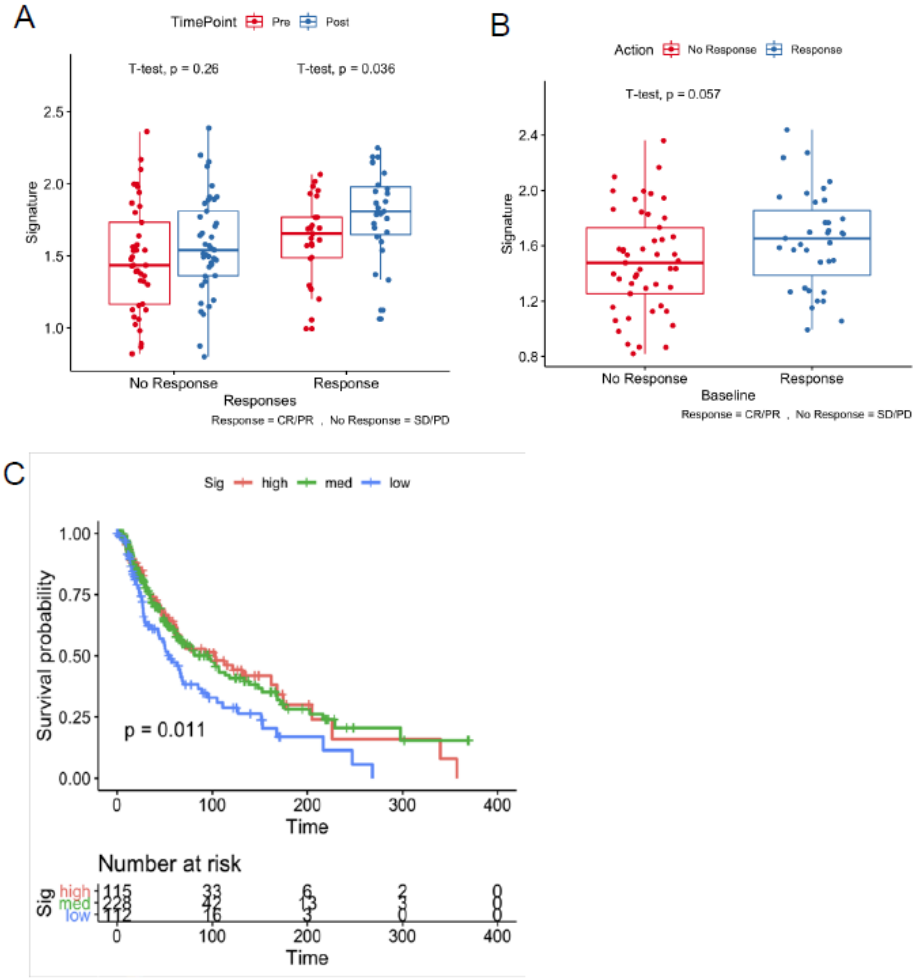

Figure 9. Survival plots based on the analysis of MLANA (D), MITF (E) and AXL (F). Analysis of the baseline biopsy samples (n = 84) of patients treated with nivolumab with or without ipilimumab in CheckMate 038. The graphs separate the upper and lower quartile of the log2 FPKM of each gene.

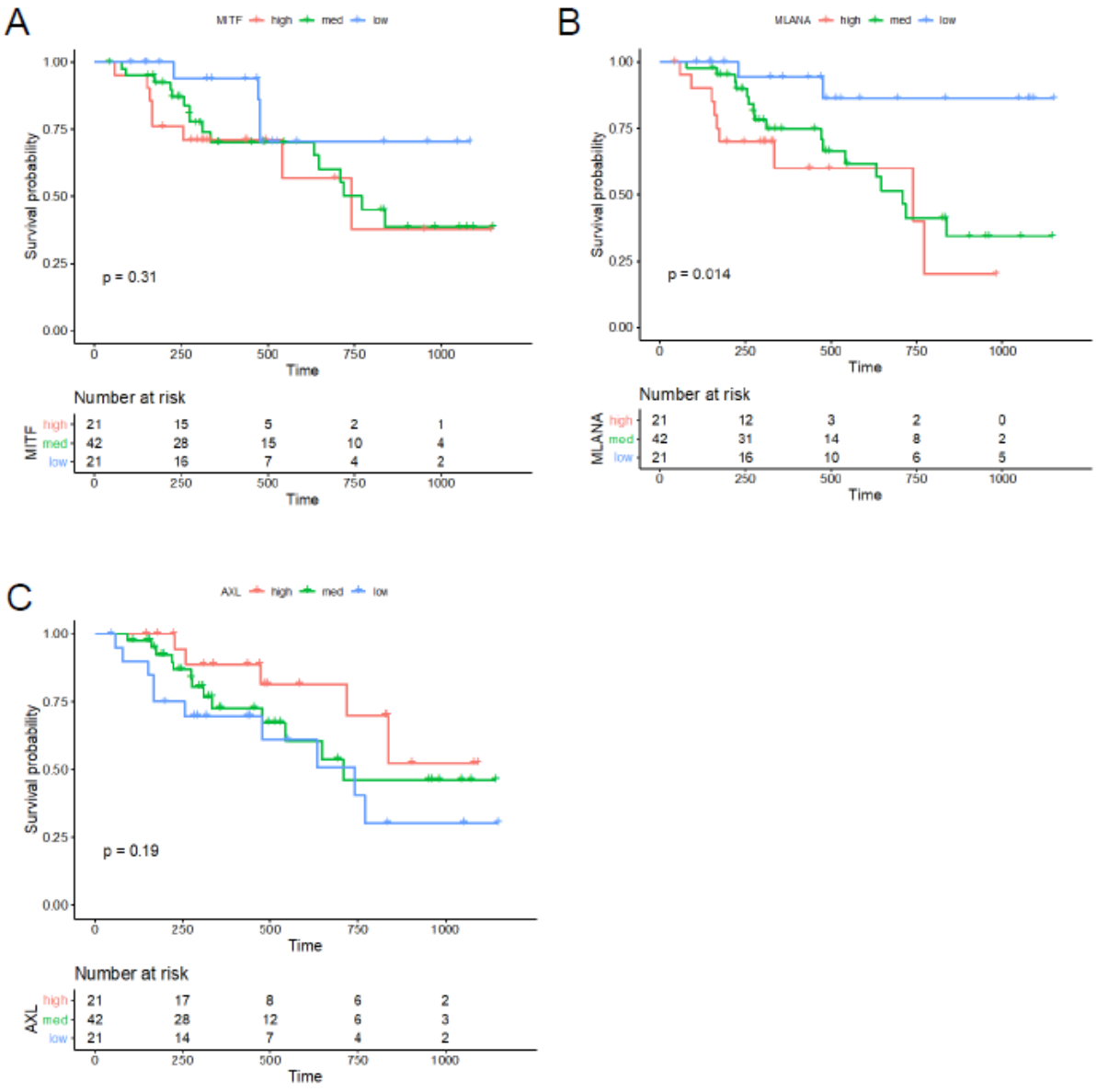

List of Supplementary Materials

Supplemental Figures

Supplemental Figure 1. IFNγ and TNF drive loss of MART-1 and gain of NGFR expression in baseline differentiated cell lines and baseline differentiation status of cell lines is not governed by their mutation status. A) Flow cytometry plots of baseline differentiated cell lines (left) and baseline undifferentiated cell lines (right) upon IFNγ or TNF exposure. B) Mutation status of the eight cell lines for select relevant genes.

Supplemental Figure 2. A) PCA of gene expression on all genes. B) Signature score of each sample based on genes in "GO_Interferon-gamma mediated signaling pathway" shows all samples upregulated IFNγ-related response genes. C) TNF samples (left) for IFNγ signature genes. D) IFNγ samples (right) for TNF signature genes.

Supplemental Figure 3. A) K-means clustering of the induced ATAC-seq peaks, with their positions relative to the transcriptional start sites. B) Top enriched motifs in the hyperaccesible ATAC peaks of TNF- and IFNγ-exposed cell lines.

Supplemental Figure 4. A-B) VIPER analysis plots showing inferred TF activity for differentiated versus undifferentiated lines for (A) TNF or (B) IFNγ. C-D) TNF and IFNγ comparisons of each baseline differentiation status.

Supplemental Tables

Supplemental Table 1. Gene expression loadings.

Supplemental Table 2. Gene set enrichment analysis results.